

# **A point mutation in HIV-1 integrase redirects proviral integration into centromeric repeats**

Shelby Winans<sup>a,b,c</sup> and Stephen P. Goff<sup>a,b,c#</sup>

<sup>a</sup>Department of Biochemistry and Molecular Biophysics

Columbia University Medical Center, New York, NY

<sup>b</sup>Department of Microbiology and Immunology

Columbia University Medical Center, New York, NY

<sup>c</sup>Howard Hughes Medical Institute, Columbia University, New York, NY

#Lead Contact: address correspondence to Stephen P. Goff, [spg1@cumc.columbia.edu](mailto:spg1@cumc.columbia.edu)

1 **Abstract**

2 Retroviruses utilize the viral integrase (IN) protein to integrate a DNA copy of their  
3 genome into the host chromosomal DNA. HIV-1 integration sites are highly biased towards  
4 actively transcribed genes, likely mediated by binding of the IN protein to specific host  
5 factors, particularly LEDGF, located at these gene regions. We here report a dramatic  
6 redirection of integration site distribution induced by a single point mutation in HIV-1 IN.  
7 Viruses carrying the K258R IN mutation exhibit more than a 25-fold increase in integrations  
8 into centromeric alpha satellite repeat sequences, as assessed by both deep sequencing and  
9 qPCR assays. Immunoprecipitation studies identified host factors that uniquely bind to the  
10 mutant IN protein and thus may account for the novel bias for integration into centromeres.  
11 Centromeric integration events are known to be enriched in the latent reservoir of infected  
12 memory T cells, as well as in patients who control viral replication without intervention (so-  
13 called elite controllers). The K258R point mutation in HIV-1 IN reported in this study has  
14 also been found in databases of latent proviruses found in patients. The altered integration  
15 site preference induced by this mutation has uncovered a hidden feature of the  
16 establishment of viral latency and control of viral replication.

17

18 Word count: 201

19

20

21

22

23

24 **Main**

25

26           Insertion of the viral DNA genome into the host cell genome, a process termed  
27 integration, is an obligate step of a successful retroviral infection. By permanently  
28 integrating the viral genome into the host genome, retroviruses are able to persist  
29 indefinitely in the infected cell as a provirus. Integration is solely catalyzed by the virally  
30 encoded integrase (IN) protein<sup>1,2</sup>. Although all of the host genome is available as a target for  
31 integration at some frequency, the distribution of integration sites across the genome is not  
32 completely random<sup>3-5</sup>, and various retroviruses exhibit distinct integration site  
33 preferences<sup>6</sup>. Specifically, human immunodeficiency virus (HIV-1) has a preference for  
34 integrating into active gene regions<sup>7</sup>. Differential integration site selectivity can be primarily  
35 explained by the binding of the viral IN protein to various host factors<sup>8</sup>. The preference for  
36 HIV-1 to integrate into active genes for instance was found to be in part due to binding of the  
37 IN protein to the host factor LEDGF, a general transcriptional activator<sup>9-12</sup>. These host factors  
38 are believed to act largely as bimodal tethers, binding both the viral IN protein and host  
39 chromatin, and thereby biasing integration sites to specific genomic regions<sup>13</sup>.

40           Integration targeting by chromatin tethering is a conserved mechanism amongst  
41 retroviruses and retrotransposons alike. The yeast Ty elements in particular exhibit highly  
42 specific integration targeting, down to the nucleotide in some cases<sup>14</sup>. Ty5 elements are  
43 mainly integrated into heterochromatic regions such as telomeres or the mating type loci  
44 through interaction of the Ty5 IN protein with the yeast silencing factor Sir4<sup>15,16</sup>. The affinity  
45 of Ty5 IN for Sir4 is dependent on phosphorylation of the targeting domain of IN<sup>17</sup>. In the  
46 absence of IN phosphorylation, as occurs during certain stress conditions, Sir4 binding is lost

47 and Ty5 integration is dramatically redirected in a dispersed fashion throughout the yeast  
48 genome<sup>17</sup>.

49 HIV-1 IN is known to be heavily post-translationally modified, but no evidence to date  
50 has linked any post-translational modifications (PTMs) to integration site selection<sup>18,19</sup>.  
51 There are four major acetylation sites in the C-terminal domain (CTD) of HIV-1 IN (K258,  
52 K264, K266 and K273)<sup>20,21</sup>. We mutated these lysine residues to charge-conservative  
53 arginines, either singly or in combination. We generated pseudotyped single-round infection  
54 HIV-1 viral reporter constructs expressing luciferase, packaged into virion particles with  
55 either a WT IN or a mutant IN, and used them to transduce cells in culture. Infected cells were  
56 collected at 48 hours post-infection and assayed for successful viral transduction by  
57 quantifying viral DNA products as well as luciferase activity (Fig. 1). We have previously  
58 reported the effects of these mutations on viral transduction, and that mutation of all  
59 acetylated lysine residues in combination led to a dramatic decrease in proviral transcription  
60 immediately after viral DNA integration<sup>22</sup>. In this study, we focus specifically on the K258R  
61 point mutation in HIV-1 IN.

62 The K258R point mutation in IN caused a modest 3-fold defect in total reverse  
63 transcription (RT) as gauged by qPCR quantification of viral DNAs (Fig. 1A), and an equally  
64 modest 2-fold decrease in the abundance of 2-LTR circular DNA, a structure generated upon  
65 nuclear entry (Fig. 1B). The mutation resulted in a similar 2-fold reduction in the levels of  
66 proviral DNA formed after infection as compared to WT, measured by qPCR amplification of  
67 host-viral junctions (so-called Alu-gag assays; Fig. 1C). Quantification of luciferase activity  
68 and steady state viral mRNA transcripts corroborated a modest decrease in overall viral  
69 transduction (Fig. 1D-E). These findings indicate that all viral DNA intermediates and viral

70 mRNA levels are reduced by a comparable amount in the cells infected with virus carrying  
71 the K258R IN mutation, and that there is no significant defect at the step of integration. The  
72 small decrease in transduction is accounted for by the initial decrease in reverse  
73 transcription products and thus in viral DNA available for subsequent steps.

74         Based on the alteration of integration site distribution induced by changes in  
75 phosphorylation status of the retrotransposon Ty5 IN in yeast, we mapped integration sites  
76 produced by the acetylation mutant INs as compared to WT IN. We used PCR and high-  
77 throughput DNA sequencing methods to recover and characterize viral-host genome  
78 junctions. Integrations were then mapped to unique human sequences using Bowtie2 and  
79 analyzed for correlation with RefSeq genes, CpG islands, transcription start sites, DNase  
80 hypersensitivity sites and various protein or histone binding sites identified in ChIP-seq  
81 datasets. These alignments are restricted to single- or low-copy number genomic sequence  
82 databases.

83         The combinatorial quadruple acetylation (QA) mutant IN and three of the four point  
84 mutant INs produced proviral integration patterns with very little deviation from WT  
85 pattern (Fig. S1). However, we observed significant differences in the distribution of  
86 proviruses integrated at uniquely mapped sequences by the K258R mutant IN as compared  
87 to those formed by WT IN (Fig. 2, Table 1). As previously shown, WT HIV-1 proviruses were  
88 preferentially located in and around annotated RefSeq genes. The K258R mutation reduced  
89 this preference for integration into genes to the level of random chance (matched random  
90 control, MRC) (Fig. 2A). Similarly, the WT IN showed the expected slight preference for  
91 integrating near CpG islands, but the K258R mutant IN showed less of this preferential  
92 targeting (Fig. 2B). This general reduction in integration frequency near these sites held true

93 for other genomic features as well, including DNase hypersensitivity regions and RNA  
94 polymerase II binding sites (Fig. 2C-D). These decreases were not due to an overall decrease  
95 in integration frequency, since all quantifications were normalized to the total number of  
96 unique integrations mapped. The distribution of integration sites relative to transcription  
97 start sites, however, was unchanged by the K258R mutation (Fig. 2E). We also correlated  
98 proviral integration sites to the genomic coordinates of various pre-infection histone  
99 modifications present in HeLa cells (Fig. 2F). We observed no notable differences in the  
100 frequency of proviral integration sites occurring in proximity to any of four chromatin  
101 modifications (H3K27ac, H3K36me3, H3K4me3 and H3K9me3) generated by the K258R  
102 mutant IN as compared to WT (Fig. 2F).

103         The analysis of the distribution of integrations of mutant K258R IN into unique  
104 mappable sites showed a loss of selective targeting to active genes as well as other features,  
105 but did not reveal a concomitant increase in integration frequency elsewhere. To examine  
106 the distribution of integration sites more globally and determine where the K258R mutant  
107 IN is being redirected, we made use of scan statistics to identify regions of the genome with  
108 high numbers of viral integrations in an unbiased fashion, and specifically including highly  
109 repetitive sequences<sup>23</sup>. We analyzed common sites of integration or “hot-spots” using the  
110 custom perl script<sup>24,25</sup>. This script first removes identical reads resulting from potential PCR  
111 duplication. Reads with identical viral-host genome junction sequences but disparate read  
112 lengths (breakpoints) were condensed into a single event. To account for potential copying  
113 errors induced by multiple rounds of PCR or sequencing we also combined those  
114 integrations in which the host sequence had >95% similarity over the length of the read. We

115 then used a sliding window to scan the human genome for common sites of integration. For  
116 our purposes hot-spots were defined as 5 or more integrations in a 10 kb window.

117 We identified an unprecedented number of hot-spot sites for integration by the  
118 K258R mutant IN that all clustered in centromeres (Table 2). The frequency of insertion of  
119 the mutant into centromeric regions was extraordinarily high, with 10 clear genomic hot  
120 spots of integration. There were no such detectable integration hot-spots in cells infected  
121 with WT HIV-1 virus. WT HIV-1 IN has been previously reported to disfavor integration into  
122 centromeric repeats with on average less than 1% of detectable proviruses found in or near  
123 centromeres<sup>7,26</sup>. The clustering we observe in the K258R mutant integration distribution  
124 could not be attributed to selective outgrowth of the infected cells in the population as the  
125 samples were collected only 48 hours post-infection.

126 To better quantify all integration events in centromeric regions, we extracted  
127 genomic coordinates of centromeres from the hg38 human reference genome and  
128 determined the distance from each integration to the nearest centromere. In agreement with  
129 the hot-spot analysis, we found a dramatic increase in integration frequency in centromeric  
130 regions specifically for proviruses integrated by the K258R mutant IN as compared to WT  
131 (Fig. 3A). We found that an average of 28% of the proviruses integrated by the K258R mutant  
132 IN occurred into centromeres. Again, we detect less than 1% of the proviruses integrated by  
133 a WT IN in centromeres, below even what is expected by random chance. The observed  
134 preference of K258R is specific for centromeric sequences, and we did not observe an  
135 increase in integration in the flanking peri-centromeric region (Fig. 3B).

136 We also analyzed the integration sites generated from the other acetylation mutant  
137 IN proteins. On average 1.7 – 4% of the detected proviruses integrated by these mutant IN

138 proteins were detected in centromeric regions, a 2-4 fold increase as compared to WT (Fig.  
139 3A). Thus, while all mutants exhibited a slight increase in preferential targeting to the  
140 centromeres, the K258R mutation alone strongly retargeted integration into centromeres at  
141 a shockingly high frequency, indicating that the effect of the K258R mutation in IN is unique  
142 to this residue, and not a general feature of blocking IN acetylation.

143         It should be noted that the magnitude of the observed phenotype in the NGS analysis  
144 was highly variable between independent replicate experiments. The fraction of the total  
145 integrations mediated by the K258R mutant IN recovered in centromeric regions ranged  
146 from extraordinarily high (~80% -- the vast majority of integrations) to only moderately  
147 high (6% and 1%), but the proportion was consistently much higher than seen with the WT  
148 IN. To document this variability, we plotted the absolute value of the residuals from the mean  
149 observed in each replicate sequencing run for WT as well as in all IN mutants (Fig. 3C). The  
150 K258R mutation in IN produces a broad range of centromeric integration frequencies  
151 whereas WT IN and other IN mutant viruses gave a tight, uniform distribution around the  
152 mean in all trials. The potential for dramatically increased centromeric integration is a  
153 unique attribute of the K258R mutant IN.

154         The large variability of the observed integration targeting phenotype is likely  
155 attributable to how repetitive DNAs are sequenced and/or mapped. Traditional  
156 bioinformatics tools to map sequence data to the genome are limited in their capacity to deal  
157 with repetitive sequences, and many repeat elements are not even present in genome  
158 assemblies because they cannot be accurately placed. For this reason many integration site  
159 mapping studies to date focus exclusively on uniquely mapped reads to avoid the  
160 complexities of handling reads that map to multiple sites (“multi-mapping reads”). Our



161 sequencing reads were mapped using a stringent Bowtie2 end-to-end alignment algorithm,  
162 with conservative reporting options that likely underestimate the true frequency of  
163 utilization of repetitive DNA as targets for integration. To obtain independent confirmation  
164 of the striking retargeting, we made use of several other bioinformatics tools commonly used  
165 in the field to re-analyze our integration site sequencing data.

166 We first confirmed this preference of the K258R mutant IN for integrating into  
167 centromeres using a Bowtie2-based sensitive local alignment strategy which allows for “soft-  
168 clipping” or omission of characters from the ends of reads in order to achieve the best  
169 alignment score. This can be advantageous if adaptor and/or viral sequences were not fully  
170 removed from the ends of reads in initial analysis steps but is in general a less conservative  
171 mapping approach. We further validated the centromeric integration preference of the  
172 K258R mutant IN using the BLAT mapping algorithm<sup>27</sup>, which is more commonly used  
173 amongst published integration site analysis studies. The BLAT mapping algorithm is based  
174 on BLAST and similarly reports all valid alignments above a set threshold score regardless  
175 of whether a read is unique or multi-mapping to repetitive sequences. Regardless of mapping  
176 algorithm, the data show that the K258R mutation in IN results in a dramatic redirection of  
177 integrations towards centromeres (Fig. S2). This site bias is not seen in any of the replicate  
178 tests of WT IN or other acetylation mutant IN proteins.

179 While the initial integration site mapping indicated that the K258R IN mutation  
180 induces a preference for integrating into centromeric regions, these algorithms do not  
181 identify specific target sequences and in fact do not even consider integration into the vast  
182 majority of repetitive sequences, which are largely excluded from the human reference  
183 genome. Centromeres are composed of tandem repeats, including both very short unit length

184 repeats, and a high proportion of so-called alpha satellite sequence DNA comprised of  
185 alphoid repeats with a unit length of approximately 171 bp<sup>28</sup>. A number of other satellite  
186 sequences are present at lower abundance in the centromeric regions as well<sup>26,29,30</sup>. To  
187 determine which class of repeats may be specifically targeted by the K258R mutant IN,  
188 sequencing reads were mapped directly to the RepeatMasker track from the UCSC Genome  
189 Browser<sup>31</sup>. The RepeatMasker track includes all known repetitive sequences present in the  
190 genome, including simple repeats and shorter repeat units that are not present in the  
191 reference genome assembly. This allowed us to quantify integrations into all known  
192 repetitive regions, both in the centromere and outside, as well as obtain information on the  
193 repeat classes that are preferred targets of integration.

194 The K258R IN mutation causes a specific targeting of integrations into alphoid repeat  
195 sequences (Fig. 4A). This preference for alphoid repeats is not seen with WT IN or other  
196 acetylation mutant IN proteins, and indeed alpha satellite DNA specifically has been  
197 previously reported to be a disfavored target of WT HIV-1 integration<sup>26</sup>. The frequency of  
198 integrations into other common repeat classes such as Alu and L1 elements were not  
199 significantly different between WT and mutant INs (Fig. 4B). The K258R mutation of IN  
200 seems to uniquely redirect integrations to alpha satellite repetitive DNA and not other  
201 classes of repeat sequences.

202 For all integrations by the K258R mutant IN that mapped to the centromere, we  
203 extracted the immediate flanking host genome sequences (10 bp upstream and 10 bp  
204 downstream), removed all identical junctions to be conservative and then aligned these to  
205 the alphoid repeat consensus sequence (AJ131208.1). We observe highly selective sites of  
206 insertion within the alpha satellite sequence by the K258R mutant IN protein, with two

207 preferred spots of integration at nucleotide position 13 and 133 in the alphoid consensus  
208 sequence (Fig. 4C). The best alignment for the viral-host junction sequences at each hot spot  
209 was identical to the base position, but notably the host sequences at all the junctions were  
210 distinct, and thus represented distinct members of the alphoid repeat family. Thus, the many  
211 insertions into the alpha repeats are truly independent integration events. These two  
212 preferred sites in the repeat do not share a high level of sequence identity. There are no  
213 known protein binding motifs near either of the preferred sites. It is thus unclear why either  
214 of these two sequences is a preferred hot-spot for the mutant IN.

215         Due to the variability in the magnitude of the phenotype as well as the limitations of  
216 deep sequencing and available analytic tools, we wanted to verify the observed altered  
217 integration site distribution using a second method. In a modification of the Alu-gag method  
218 to quantify integration frequency, we devised a nested PCR approach to specifically assay for  
219 integrants in centromeric repeats. We replaced the primer located in the Alu repeat element  
220 that is typically used in Alu-gag assays with primers complementary to the alphoid repeat  
221 consensus sequence<sup>26,32</sup>. We utilized two unique alphoid primers in our assay. To analyze  
222 both the 5' and 3' ends of the provirus we used primers complementary to either gag or  
223 luciferase respectively. This allowed for four unique combinations of primers in the first  
224 round of PCR that would selectively amplify proviruses in or near centromeric alphoid  
225 repeats. A subsequent second round quantitative PCR, using LTR specific primers, reported  
226 the yield of amplified viral DNA. The assays revealed a dramatic increase in the frequency of  
227 centromeric integration events for proviruses integrated by the K258R mutant IN (Fig. 5A).  
228 The magnitude of the effect was again highly variable, both between primer combinations  
229 and within a given primer pair, but was always dramatic. The K258R mutant IN increased

230 integration frequency near centromeric alphoid repeats over the wild-type control by an  
231 average of 30-400 fold. The alpha satellite bias was again only seen with the K258R mutant.  
232 All other mutations blocking other acetylation sites displayed a similar level of centromeric  
233 integrations as wild type controls.

234 In our initial analysis to identify common sites of integration from NGS data, the  
235 identified genomic hot spots were all found in only a subset of chromosomes (Table 2). To  
236 determine whether the K258R mutant IN displayed any particular chromosomal preference,  
237 we also performed a qPCR assay utilizing chromosome-specific non-repetitive centromere  
238 primers to quantify specific centromeric DNA content present at the LTR-host genome  
239 junction. Shown are some representative examples using chromosome-specific primers for  
240 chromosomes 1, 2, 4 and 14 (Fig. 5B-E). The K258R mutant virus was observed to integrate  
241 much more frequently than WT or any other acetylation IN mutant viruses at sites near the  
242 centromeres regardless of chromosome. The apparent bias for some chromosomes that we  
243 observed in the initial “hot spot” analysis of the NGS data could be due to gaps or  
244 discrepancies in the assignments of the centromere sequences present in the genome  
245 assembly database. The PCR data suggest that K258R virus is targeted to centromeres of  
246 many, if not all, chromosomes.

247 Because HIV-1 integration is in part targeted through host factor interactions, it is  
248 plausible that the K258R mutation in the IN protein could modulate integration site selection  
249 by mediating differential binding of a specific host factor. To test this possibility, we  
250 generated mammalian expression vectors expressing either WT or K258R mutant IN protein  
251 and tested for host binding proteins. In both cases, the IN protein was N-terminally tagged  
252 with HA for immunoprecipitation. HEK293T cells were transfected with the IN plasmids and

253 lysates were harvested after 24 hours of expression. Adequate and comparable expression  
254 of both WT and mutant IN proteins was confirmed via Western blot using both HA- and IN-  
255 specific antibodies. WT and mutant IN were immunoprecipitated and interacting host  
256 proteins were subject to mass spectrometry for identification.

257 We identified 43 and 56 proteins that bound to WT or K258R IN proteins,  
258 respectively, above the background of an empty vector control (Table 3). The majority of  
259 these host factors were shared between WT and K258R mutant IN. Based on a preliminary  
260 gene ontology analysis, the majority of factors that bind either WT or mutant IN protein are  
261 generic nucleic acid binding proteins (Table 3). Approximately a third of the 43 proteins we  
262 detected binding to WT IN have been previously reported by another mass spectrometry  
263 screen done in HEK293T cells, validating our approach<sup>33</sup>. We did not detect LEDGF in our  
264 immunoprecipitation, in agreement with previous studies that also failed to recover LEDGF  
265 in similar experiments in HEK293T cells<sup>33</sup>.

266 Mutant K258R IN bound to the majority of previously reported host factors, but  
267 several binding partners were identified as uniquely binding to the K258R mutant IN. Two  
268 factors involved in mitotic chromosome condensation (NCAPD3 and SMC4) were found to  
269 preferentially bind K258R mutant IN along with multiple components of the catalytic core of  
270 the protein phosphatase I (PPI) complex. These factors have clear links to heterochromatin  
271 formation and regulation. In addition, gene ontology analysis of the partners revealed an  
272 enrichment for genes involved in tRNA processing as well as antiviral interferon stimulated  
273 genes (Table 4). It is not immediately obvious how preferential binding of the mutant IN to  
274 these proteins would so strongly redirect integrations to centromeric regions.

275           To our knowledge, the K258R mutant shows the most dramatic retargeting of  
276 integration sites reported for any retrovirus so far. The striking redirection of integrations  
277 to the centromere caused by the K258R mutation in the IN protein is especially provocative  
278 in light of recent work linking centromeric HIV-1 integrations to viral latency and control.  
279 Proviruses in centromeric satellite DNA have been found in the latent reservoir of patients  
280 as well as associated with deep viral latency in past reactivation studies<sup>32,34</sup>. Thus,  
281 integration into these “gene deserts” promotes viral silencing and the formation of the major  
282 impediment to HIV-1 cure. More recently it has been shown that proviral sequences from  
283 elite controllers were also preferentially enriched in centromeric satellite DNA<sup>35</sup>, suggesting  
284 that a common process may underlie the resultant proviral silencing in both settings. It is  
285 not yet known whether IN mutations are associated with increased centromeric integration  
286 in patients, but we have found the K258R mutation present at low frequency in proviral  
287 sequence repositories of latent proviruses, drug resistant mutants, and from patients on  
288 suppressive antiretroviral therapy<sup>36</sup>. Understanding how this single point mutation can  
289 cause such a striking retargeting of integration will be important for characterizing and  
290 ultimately manipulating the mechanisms that underlie viral latency and long term control in  
291 patients.

292

293

294

295

296

297

## 298 **Methods**

299

### 300 **Cells and plasmids**

301 HEK293T cells and HeLa cells were cultured in DMEM media supplemented with 10%  
302 FBS and 1% pen-strep at 37°C, 5% CO<sub>2</sub>.

303 HIV-1 viral constructs were derived from the replication defective pNL4.3R-E-  
304 plasmid (NIH AIDS Reagent Program #3148) carrying a firefly luciferase reporter gene in the  
305 *nef* open reading frame. Mutations were introduced into the IN open reading frame using  
306 PCR site-directed mutagenesis with custom primer<sup>22</sup>.

### 307 **Transfection, virus preparation and infection**

308 To prepare pseudotyped virus for infection, HEK293T cells were co-transfected with  
309 the pNL4.3.Luc.R-E- viral vector as well as a plasmid expressing the vesicular stomatitis virus  
310 glycoprotein (VSV-G) envelope (pMD2.G) using Lipofectamine 3000 (Life Technologies)  
311 according to basic manufacturer's protocol. Viral supernatants were collected at 48 hours  
312 post-transfection, filtered through a 0.45 micron filter, and DNase treated to eliminate  
313 plasmid DNA contamination. Viral preparations were normalized by RNA viral genome  
314 content, diluted 3-fold with fresh culture medium and immediately used for infection of HeLa  
315 cells.

### 316 **Luciferase assay**

317 Successful viral transduction was assayed after 48 hours by measuring luciferase  
318 activity with the Promega Luciferase Assay System (Cat# E4550). Luminescence (RLU)  
319 measurements were normalized for total cell count as determined by protein concentration.

### 320 **Quantitative PCR for viral DNA intermediate and RNA analysis**

321 DNA was isolated from acutely infected cells 2 days post-infection using the Qiagen  
322 DNeasy Blood and Tissue Kit. Quantitative PCR for viral DNAs was performed using FastStart  
323 Universal SYBR Green Mastermix (Bio-Rad) according to manufacturer's protocol on ABI  
324 7500 Fast Real Time PCR System. Total viral DNA was quantified using primers  
325 complementary to the luciferase gene. Reverse transcription (RT) products were detected  
326 with LTR specific primers. 2-LTR circles were quantified as previously published and  
327 normalized to total virus<sup>37</sup>. Integrated proviruses were quantified using the published Alu-  
328 gag nested PCR protocol<sup>38,39</sup>.

329 To quantify steady state viral mRNA levels, RNA was extracted from cells using a  
330 standard Trizol protocol. Reverse transcription was performed using random hexamer  
331 primers with Maxima H Reverse Transcriptase (Thermo Fisher). Viral cDNA was then  
332 quantified via qPCR using primers complementary to spliced *tat* message and normalized to  
333 a housekeeping gene.

334 All primers used for quantification can be found in Table S1. A minimum of three  
335 biological replicates were performed per experiment with technical duplicates within each  
336 experiment for precision. Biological replicates refer to completely independent experiments,  
337 while technical replicates refer to repeated measures of the same samples. A single factor  
338 ANOVA analysis was used to identify significant changes ( $p < 0.05$ ). If appropriate, pairwise  
339 comparisons were performed using a two-tailed paired t-test assuming unequal variance.

#### 340 **Next generation sequencing (NGS) library construction**

341 DNA sequencing libraries were prepared as described previously<sup>22,25,40</sup>. Briefly, five  
342 micrograms of purified genomic DNA from infected cells was randomly sheared using a  
343 Branson 450 Digital Sonifier. Sheared ends of DNA were subsequently repaired, A-tailed and



344 ligated to custom oligonucleotide adaptors. Nested PCR was performed using viral and  
345 adaptor specific primers to enrich the library for proviral-host genome junctions and add  
346 necessary index and flow cell attachment sequences for Illumina (See Table S2 for library  
347 adaptor and primer sequences). PCRs were performed such that the final library product  
348 should contain 40 bp of the 3' viral LTR sequence immediately prior to the junction with the  
349 host genome sequence. Sequencing was performed using the Illumina MiSeq platform. Three  
350 unique biological replicate libraries were generated and sequenced independently.

### 351 **Integration site mapping data analysis**

352 Reads were initially demultiplexed by unique dual barcodes and filtered to exclude  
353 reads not containing an initial viral LTR sequence at the host junction using a custom python  
354 script<sup>22</sup>. We required an exact match to the terminal 40 nt of the 3' viral LTR. All reads were  
355 then trimmed to remove both leading viral sequence as well as any residual adaptor  
356 sequences. Reads of less than 20 nucleotides after all filtering steps were discarded.  
357 Remaining reads were mapped to the GRCh38 human genome using either Bowtie2 or BLAT  
358<sup>27,41</sup>.

359 For majority of analyses, unless otherwise noted, reads were first aligned to the  
360 pNL4.3.Luc.R-E- vector genome to remove any viral auto-integration or circular products.  
361 The remaining reads were then aligned to the unmasked GRCh38 human reference genome  
362 using Bowtie2 end-to-end alignment with a seed length of 28 nucleotides and a maximum of  
363 2 mismatches permitted in the seed. Reads that mapped to multiple locations were not  
364 suppressed. Instead, best alignment was reported. For reads with equally good alignments,  
365 one of the alignments was reported at random.

366           Where noted, sequences were further locally aligned to the unmasked GRCh38  
367 genome build using either Bowtie2 sensitive local settings or BLAT. For BLAT analysis,  
368 alignments were filtered for 95% minimum identity and a minimum score of 30. All  
369 acceptable alignments above this threshold were reported with scores based on number of  
370 matched/mismatched bases and a default gap penalty. For reads mapping to multiple  
371 locations equally well, all alignments were reported. Parameters for Bowte2 local mapping  
372 were 20 nt seed length, allowing 0 mismatches in the seed.

373           Reads were also aligned directly to the RepeatMasker genome track from UCSC using  
374 the same mapping algorithms. Only data from Bowtie2 local mapping is shown here. The  
375 RepeatMasker track contains all annotated repeat sequences in the human genome <sup>31</sup>.  
376 Number of integrations falling into each specified repeat class was calculated and presented  
377 as a percent of the total number of integrations mapped.

### 378 **Hot-spot analysis of viral integrations**

379           Using a previously reported custom perl script, common sites, or “hot-spots”, of viral  
380 integration were determined <sup>42,43</sup>. First, identical reads, or PCR duplicates were condensed.  
381 Second, reads with identical junctions but varying sonication breakpoints were condensed  
382 to eliminate any confounding effects of clonal expansion. To be stringent, reads with highly  
383 similar sequences (i.e. >95% identity) were also combined to eliminate any artifacts  
384 produced from small PCR or sequencing errors. From here, “hot-spots” of viral integration  
385 were determined using a sliding window approach <sup>23</sup>. This script searches for multiple  
386 integrations falling within a set range of nucleotides from each other. For this study “hot-  
387 spots” were defined as regions of 10 kb or less with five or more unique viral integrations.

### 388 **Analysis of integration sites with respect to genomic annotations**

389           Genomic coordinates of annotated RefSeq genes, transcription start sites, CpG islands  
390 and DNase hypersensitivity regions were extracted from the GRCh38 genome assembly via  
391 the UCSC Genome Browser. The genomic coordinates of centromeric sequences were also  
392 extracted from UCSC Genome Browser. Locations of RNA polymerase II binding sites and  
393 histone modifications were extracted from ENCODE data sets generated from uninfected  
394 HeLa cells (Pol II: ENCFF246QVY; H3K27Ac: ENCFF113QJM ; H3K9me3: ENCFF712ATO ;  
395 H3K36me3: ENCFF864ZXP ; H3K4me3: ENCFF862LUQ). Distance of proviral integrations to  
396 nearest feature was calculated using BedTools <sup>44</sup>. A matched random control (MRC) data set  
397 of comparable size was generated with BedTools Random command and mapped in parallel  
398 to experimental data sets.

399           A one-sample t-test was used to compare integration distribution between  
400 experimental samples and MRC (Table S3). To gauge the statistical significance of differences  
401 in integration patterns between WT IN and mutant IN we used a paired t-test of three  
402 independent replicate data sets for each condition or Fisher's exact test on the aggregate  
403 integration data (Table S4).

#### 404 **Sequence analysis of centromeric integration sites**

405           The host sequence flanking the site of integration was extracted from Bed coordinates  
406 of mapped integration sites. To align sites of integration along the repeat length of the  
407 alphoid repeat, we used only the 5 base pairs flanking the site of integration (total length 10  
408 bp) to align to a consensus sequence for the alphoid repeat monomer (AJ131208.1). Only  
409 unique junctions were aligned. Alignments were performed with Clustal Omega <sup>45</sup>. For count  
410 purposes, we defined 17 bins spanning the alphoid repeat monomer, each consisting of ten  
411 base pairs, and counted the number of integrations falling in each bin.

## 412 **PCR assays for quantifying centromeric integrations**

413 To determine if centromeric DNA sequences were over-represented in library  
414 preparations, we made use of previously reported unique chromosome specific centromere  
415 primers<sup>46</sup>. Amplified viral-host genome fragments from library preparations were used in a  
416 qPCR assay using centromere specific primers to relatively compare quantities of  
417 centromeric DNA sequences between infections with viruses carrying WT or mutant IN  
418 proteins.

419 To look more generically at integration into all centromeres, we devised a nested PCR  
420 assay based on both the basic Alu-gag PCR protocol for quantifying proviral integration and  
421 a previously published assay using alpha satellite specific primers (alphoid-1, alphoid-2)<sup>26</sup>.  
422 For the first nest, one of two primers complementary to the alpha satellite consensus  
423 sequence were used in conjunction with either a 5' viral specific primer (5'-gag) or a 3' viral  
424 specific primer (3'-luc). For validation purposes, a number of randomly selected fragments  
425 were cloned from the first rounds of PCR and sequenced by Sanger sequencing to verify that  
426 we were indeed amplifying alphoid repeats at the viral-host genome junction. LTR-specific  
427 primers were then used for the second nest quantitative PCR. These values were normalized  
428 to total LTR content in original unamplified DNA. See Table S1 for primer sequences used.

## 429 **Co-immunoprecipitation of IN proteins and mass spectrometry**

430 Either WT HIV-1 IN or IN harboring the K258R mutation was cloned into a  
431 mammalian expression vector (pJET). Both proteins had an N-terminal HA-tag for  
432 immunoprecipitation. As a negative control, we also transfected cells with an empty HA-  
433 vector. Constructs were transfected into HEK293T cells as described. After 24 hours, cells  
434 were collected, washed and lysed with an NP-40 lysis buffer (20 mM Tris HCl, pH 8; 137 mM

435 NaCl, 2 mM EDTA and 1% NP-40). Adequate, comparable expression of WT and mutant IN  
436 proteins was confirmed via Western blot using HA-specific or IN-specific antibodies.

437 Cell lysates were subsequently mixed with BSA blocked HA-coated magnetic beads  
438 (Pierce) and rotated overnight at 4°C. Beads were washed three times with lysis buffer,  
439 finished with two PBS washes and sent for mass spectrometry analysis (Rockefeller Mass  
440 Spectrometry Core Facility).

441 MS results were filtered by number of peptides detected vs. an empty HA vector  
442 control. Only proteins with five or more spectral counts were considered. Proteins were  
443 considered enriched when there was a minimum of 5-fold more unique spectral counts  
444 detected in the IN immunoprecipitation vs. the control precipitation. Enriched peptides  
445 immunoprecipitated by WT and K258R mutant IN were further subjected to gene ontology  
446 analysis performed with gProfiler software <sup>47</sup>.

447

#### 448 **Data and code availability**

449 Sequencing reads generated as part of this study are available at the NCBI Sequencing Read  
450 Archive: XXXX. Code uniquely generated for this analysis is available upon request.

451

#### 452 **Acknowledgements**

453 This study was supported by NCI grant R01 CA 30488 from the National Cancer Institute  
454 (S.P.G) and NIAID Ruth L. Kirschstein NRSA fellowship F32 AI 149989 from the National  
455 Institute of Allergy and Infectious Disease (S.W.). S.P.G. is an Investigator of the Howard  
456 Hughes Medical Institute.

457

458 **Author contributions**

459 Conceptualization and methodology: SW and SPG; Data curation, formal analysis and  
460 visualization: SW; Supervision, project administration and resources: SPG; Funding  
461 acquisition: SW and SPG; Writing – original draft: SW; Writing - review and editing: SPG and  
462 SW

463

464 **Additional Information**

465 Supplementary Information is available for this paper.

466 Correspondence and requests for materials should be addressed to Stephen P. Goff  
467 ([spg1@cumc.columbia.edu](mailto:spg1@cumc.columbia.edu)).

468

469 **Ethics declarations**

470 The authors declare no competing interests.

471

472 **References**

- 473 1. Bowerman, B., Brown, P. O., Bishop, J. M. & Varmus, H. E. A nucleoprotein complex  
474 mediates the integration of retroviral DNA. *Genes Dev.* **3**, 469–478 (1989).
- 475 2. Brown, P. O., Bowerman, B., Varmus, H. E. & Bishop, J. M. Retroviral integration:  
476 Structure of the initial covalent product and its precursor, and a role for the viral IN  
477 protein. *Proc. Natl. Acad. Sci. U. S. A.* **86**, 2525–2529 (1989).
- 478 3. Bor, Y. C., Bushman, F. D. & Orgel, L. E. In vitro integration of human  
479 immunodeficiency virus type 1 cDNA into targets containing protein-induced bends.  
480 *Proc. Natl. Acad. Sci. U. S. A.* **92**, 10334–8 (1995).

- 481 4. Craigie, R., Fujiwara, T. & Bushman, F. The IN protein of Moloney murine leukemia  
482 virus processes the viral DNA ends and accomplishes their integration in vitro. *Cell*  
483 **62**, 829–837 (1990).
- 484 5. Brown, P. O., Bowerman, B., Varmus, H. E. & Bishop, J. M. Correct integration of  
485 retroviral DNA in vitro. *Cell* **49**, 347–356 (1987).
- 486 6. Mitchell, R. S. *et al.* Retroviral DNA integration: ASLV, HIV, and MLV show distinct  
487 target site preferences. *PLoS Biol.* **2**, E234 (2004).
- 488 7. Schröder, A. R. W. *et al.* HIV-1 integration in the human genome favors active genes  
489 and local hotspots. *Cell* **110**, 521–9 (2002).
- 490 8. Debyser, Z., Christ, F., De Rijck, J. & Gijssbers, R. Host factors for retroviral integration  
491 site selection. *Trends Biochem. Sci.* **40**, 108–16 (2015).
- 492 9. Ciuffi, A. *et al.* A role for LEDGF/p75 in targeting HIV DNA integration. *Nat. Med.* **11**,  
493 1287–9 (2005).
- 494 10. Llano, M. *et al.* An essential role for LEDGF/p75 in HIV integration. *Science (80-. )*.  
495 **314**, 461–4 (2006).
- 496 11. Maertens, G. *et al.* LEDGF/p75 is essential for nuclear and chromosomal targeting of  
497 HIV-1 integrase in human cells. *J. Biol. Chem.* **278**, 33528–33539 (2003).
- 498 12. McNeely, M. *et al.* In vitro DNA tethering of HIV-1 integrase by the transcriptional  
499 coactivator LEDGF/p75. *J. Mol. Biol.* **410**, 811–830 (2011).
- 500 13. Kvaratskhelia, M., Sharma, A., Larue, R. C., Serrao, E. & Engelman, A. Molecular  
501 mechanisms of retroviral integration site selection. *Nucleic Acids Res.* **42**, 10209–25  
502 (2014).
- 503 14. Lesage, P. & Todeschini, A. L. Happy together: The life and times of Ty

- 504 retrotransposons and their hosts. *Cytogenetic and Genome Research* vol. 110 70–90  
505 (2005).
- 506 15. Zou, S., Ke, N., Kim, J. M. & Voytas, D. F. The *Saccharomyces* retrotransposon Ty5  
507 integrates preferentially into regions of silent chromatin at the telomeres and mating  
508 loci. *Genes Dev.* **10**, 634–645 (1996).
- 509 16. Xie, W. *et al.* Targeting of the Yeast Ty5 Retrotransposon to Silent Chromatin Is  
510 Mediated by Interactions between Integrase and Sir4p. *Mol. Cell. Biol.* **21**, 6606–6614  
511 (2001).
- 512 17. Dai, J., Xie, W., Brady, T. L., Gao, J. & Voytas, D. F. Phosphorylation Regulates  
513 Integration of the Yeast Ty5 Retrotransposon into Heterochromatin. *Mol. Cell* **27**,  
514 289–299 (2007).
- 515 18. Andrade, M. D. & Skalka, A. M. Retroviral Integrase: Then and Now. *Annu. Rev. Virol.* **2**,  
516 241–264 (2015).
- 517 19. Chen, L., Keppler, O. T. & Schözl, C. Post-translational modification-based regulation  
518 of HIV replication. *Frontiers in Microbiology* vol. 9 (2018).
- 519 20. Cereseto, A. *et al.* Acetylation of HIV-1 integrase by p300 regulates viral integration.  
520 *EMBO J.* **24**, 3070–3081 (2005).
- 521 21. Terreni, M. *et al.* GCN5-dependent acetylation of HIV-1 integrase enhances viral  
522 integration. *Retrovirology* **7**, (2010).
- 523 22. Winans, S. & Goff, S. P. Mutations altering acetylated residues in the CTD of HIV-1  
524 integrase cause defects in proviral transcription at early times after integration of  
525 viral DNA. *PLOS Pathog.* **16**, e1009147 (2020).
- 526 23. Berry, C. C., Ocwieja, K. E., Malani, N. & Bushman, F. D. Comparing DNA integration



- 527 site clusters with scan statistics. *Bioinformatics* **30**, 1493–1500 (2014).
- 528 24. Justice, J. *et al.* The MET Gene Is a Common Integration Target in Avian Leukosis  
529 Virus Subgroup J-Induced Chicken Hemangiomas. *J. Virol.* **89**, 4712–4719 (2015).
- 530 25. Malhotra, S. *et al.* Selection for avian leukosis virus integration sites determines the  
531 clonal progression of B-cell lymphomas. *PLoS Pathog* **13**, (2017).
- 532 26. Carteau, S., Hoffmann, C. & Bushman, F. Chromosome Structure and Human  
533 Immunodeficiency Virus Type 1 cDNA Integration: Centromeric Alphoid Repeats Are  
534 a Disfavored Target. *J. Virol.* **72**, 4005–4014 (1998).
- 535 27. Kent, W. J. BLAT---The BLAST-Like Alignment Tool. *Genome Res.* **12**, 656–664 (2002).
- 536 28. McNulty, S. M. & Sullivan, B. A. Alpha satellite DNA biology: finding function in the  
537 recesses of the genome. *Chromosome Research* vol. 26 115–138 (2018).
- 538 29. Miga, K. H. Centromeric satellite DNAs: Hidden sequence variation in the human  
539 population. *Genes* vol. 10 (2019).
- 540 30. Hartley, G. & O’neill, R. J. Centromere repeats: Hidden gems of the genome. *Genes* vol.  
541 10 (2019).
- 542 31. Tarailo-Graovac, M. & Chen, N. Using RepeatMasker to identify repetitive elements in  
543 genomic sequences. *Current Protocols in Bioinformatics* (2009)  
544 doi:10.1002/0471250953.bi0410s25.
- 545 32. Jordan, A., Bisgrove, D. & Verdin, E. HIV reproducibly establishes a latent infection  
546 after acute infection of T cells in vitro. *EMBO J.* **22**, 1868–1877 (2003).
- 547 33. Jäger, S. *et al.* Global landscape of HIV-human protein complexes. *Nature* **481**, 365–  
548 370 (2012).
- 549 34. Lewinski, M. K. *et al.* Retroviral DNA integration: viral and cellular determinants of

- 550 target-site selection. *PLoS Pathog.* **2**, e60 (2006).
- 551 35. Jiang, C. *et al.* Distinct viral reservoirs in individuals with spontaneous control of HIV-  
552 1. *Nature* (2020) doi:10.1038/s41586-020-2651-8.
- 553 36. Foley, B. *et al.* HIV Sequence Compendium 2018. in (Theoretical Biology and  
554 Biophysics Group, Los Alamos National Laboratory, NM, LA-UR 18-25673).
- 555 37. Mandal, D. & Prasad, V. R. Analysis of 2-LTR circle junctions of viral DNA in infected  
556 cells. *Methods Mol. Biol.* **485**, 73–85 (2009).
- 557 38. Butler, S. L., Hansen, M. S. & Bushman, F. D. A quantitative assay for HIV DNA  
558 integration in vivo. *Nat. Med.* **7**, 631–4 (2001).
- 559 39. O’Doherty, U., Swiggard, W. J., Jeyakumar, D., McGain, D. & Malim, M. H. A Sensitive,  
560 Quantitative Assay for Human Immunodeficiency Virus Type 1 Integration. *J. Virol.*  
561 **76**, 10942–10950 (2002).
- 562 40. Serrao, E., Cherepanov, P. & Engelman, A. N. Amplification, next-generation  
563 sequencing, and genomic DNA mapping of retroviral integration sites. *J. Vis. Exp.*  
564 **2016**, (2016).
- 565 41. Langmead, B., Trapnell, C., Pop, M. & Salzberg, S. L. Ultrafast and memory-efficient  
566 alignment of short DNA sequences to the human genome. *Genome Biol.* **10**, R25  
567 (2009).
- 568 42. Justice, J. F., Morgan, R. W. & Beemon, K. L. Common Viral Integration Sites Identified  
569 in Avian Leukosis Virus-Induced B-Cell Lymphomas. *MBio* **6**, e01863-15 (2015).
- 570 43. Malhotra, S. *et al.* Selection for avian leukosis virus integration sites determines the  
571 clonal progression of B-cell lymphomas. *PLoS Pathog.* **13**, e1006708 (2017).
- 572 44. Quinlan, A. R. & Hall, I. M. BEDTools: A flexible suite of utilities for comparing

- 573 genomic features. *Bioinformatics* **26**, 841–842 (2010).
- 574 45. Sievers, F. & Higgins, D. G. Clustal omega, accurate alignment of very large numbers  
575 of sequences. *Methods Mol. Biol.* **1079**, 105–116 (2014).
- 576 46. Contreras-Galindo, R. *et al.* Rapid molecular assays to study human centromere  
577 genomics. *Genome Res.* **27**, 2040–2049 (2017).
- 578 47. Reimand, J., Kull, M., Peterson, H., Hansen, J. & Vilo, J. g:Profiler--a web-based toolset  
579 for functional profiling of gene lists from large-scale experiments. *Nucleic Acids Res.*  
580 **35**, W193-200 (2007).
- 581

**Table 1:** Number of unique integrations mapped (N=3 biological replicates)

|                     | WT    | K258R |
|---------------------|-------|-------|
| Unique integrations | 17636 | 18850 |
| Within RefSeq genes | 12363 | 11737 |
| TSS (5 kb)          | 3630  | 3412  |
| TSS (1kb)           | 671   | 387   |
| CpG islands (5 kb)  | 2549  | 2291  |
| CpG islands (1 kb)  | 426   | 316   |
| RNA Pol II (1 kb)   | 501   | 447   |
| DNase HS (1 kb)     | 2048  | 2018  |
| H3K27ac (1 kb)      | 1197  | 1080  |
| H3K36me3 (1 kb)     | 1656  | 1379  |
| H3K4me3 (1 kb)      | 875   | 809   |
| H3K9me3 (1 kb)      | 121   | 108   |
| Within centromeres  | 146   | 1576  |

**Table 2:** Hot-spots of integration for viruses carrying the K258R IN mutation (5+ integrations in a 10 kb window)

| Genomic coordinates       | Number of integrants |
|---------------------------|----------------------|
| Chr14: 17749223-17757726  | 5                    |
| Chr13: 17630007-17635451  | 6                    |
| Chr21: 12443946-12448362  | 6                    |
| Chr21: 12534522-12533844  | 6                    |
| Chr13: 17669962-17678635  | 7                    |
| Chr14: 18151557-18159208  | 7                    |
| Chr22: 14673032-14672354  | 8                    |
| Chr1: 125173987-125183192 | 9                    |
| Chr22: 15024034-15019610  | 9                    |
| Chr1: 143246863-143248277 | 12                   |

**Table 3:** Host proteins immunoprecipitated with WT or K258R mutant IN protein

| Sample(s) | Host protein names  |
|-----------|---|
| WT/K258R  | PRKDC, MDN1, MYBBP1A, NUP205, CAND2, GCN1, NUP188, CKMT1A, IMMT, HEATR1, IPO4, UBE3C, AIFM1, FANCI, ABCD3, ATP2A2, ABCE1, LTN1, SUCLA2, COQ8B, ATAD3C, DDX20, AFG3L2, ATAD3A, ATAD3B, RCN2, SGPL1, TYK2, SLC16A1, MCM7, TIMM50, ARF4, RRP12, PPP1CB, SLC25A10 |
| WT        | TEX10, GEMIN4, UNC45A, YME1L1, ARF5, NOP56, EIF2S2, RPL27   |
| K258R     | NUP93, JAK1, NCAPD3, GLUD1, CHCHD3, SPATA5, CAND1, TMEM209, PLEKHG4, RPP30, HACD3, ILVBL, SMC4, RPSKA4, CAD, ALDH1B1, RPN1, PPP1CC, ATP1A1, HERC5, RTCB   |

**Table 4:** Gene ontology analysis of integrase interacting host factors

| GO category   | # of proteins | P-value | Proteins   |
|---|---------------|---------|--|
| <b><i>WT (all partners)</i></b>                     |               |         |  |
| Nucleotide binding                                  | 19            | 5.4E-5  | PRKDC, MDN1, CKMT1A, AIFM1, ABCD3, ATP2A2, ABCE1, SUCLA2, COQ8B, ATAD3C, DDX20, AFG3L2, ATAD3A, ATAD3B, TYK2, MCM7, ARF4, YME1L1, ARF5   |
| <b><i>WT (unique)</i></b>                           |               |         |  |
| rRNA processing                                     | 4             | 1.7E-3  | TEX10, GEMIN4, NOP56, RPL27  |
| <b><i>K258R (all partners)</i></b>                  |               |         |  |
| Nucleotide binding                                  | 26            | 5.2E-8  | JAK1, GLUD1, SPATA5, SMC4, RPS6KA4, CAD, ALDH1B1, ATP1A1, RTCB, PRKDC, MDN1, CKMT1A, AIFM1, ABCD3, ATP2A2, ABCE1, SUCLA2, COQ8B, ATAD3C, DDX20, AFG3L2, ATAD3A, ATAD3B, TYK2, MCM7, ARF4 |
| Antiviral mechanism by IFN-stimulated genes         | 6             | 2.1E-4  | NUP93, JAK1, HERC5, NUP205, ABCE1, NUP188  |
| tRNA processing in the nucleus                      | 5             | 8.3E-4  | NUP93, RPP30, RTCB, NUP205, NUP188   |
| PTW/PP1 complex                                     | 2             | 4.9E-2  | PPP1CB, PPP1CC   |
| <b><i>K258R (unique)</i></b>                        |               |         |  |
| tRNA processing                                     | 3             | 2.3E-2  | RPP30, RTCB, NUP93   |
| ISG15 antiviral mechanism                           | 3             | 4.7E-2  | JAK1, HERC5, NUP93   |
| Meiotic chromosome condensation / condensin complex | 2             | 5.2E-3  | NCAPD3, SMC4   |

## Figures and legends

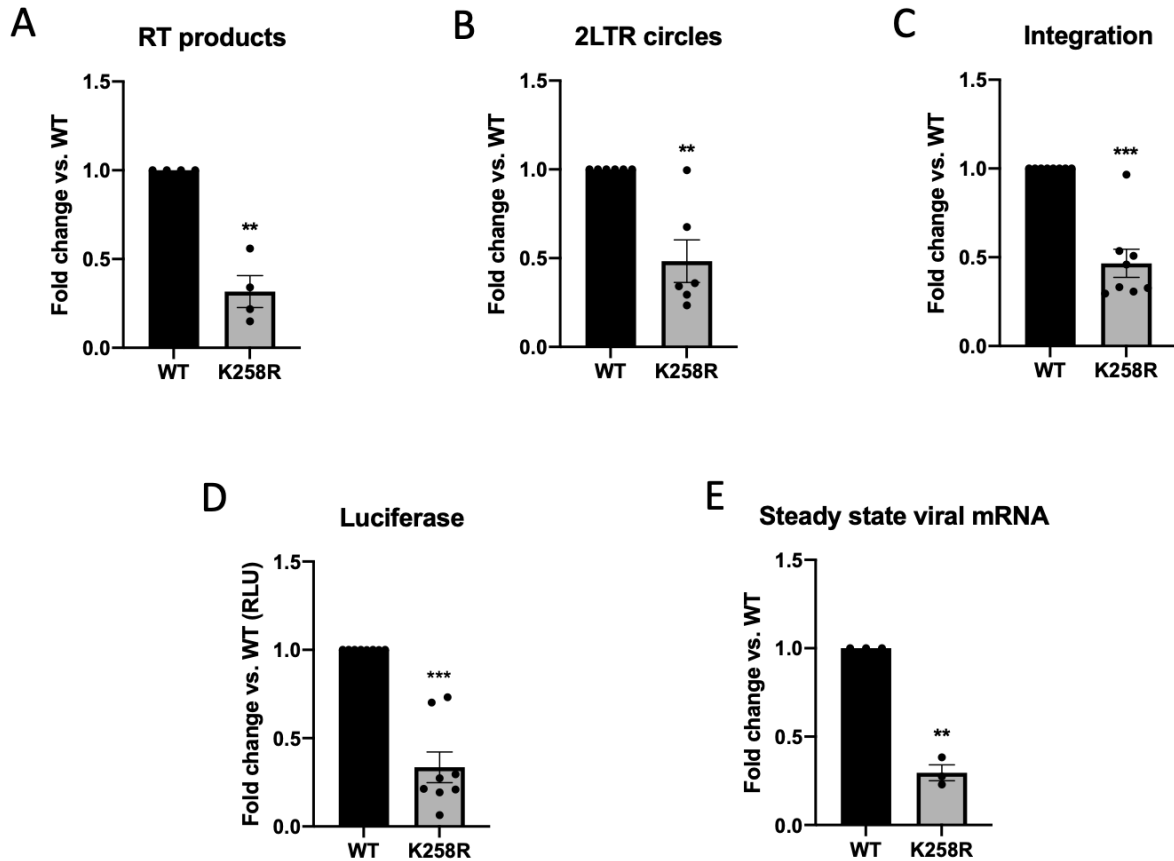


**Figure 1: K258R point mutation in HIV-1 IN has modest effects on early viral replication.** HeLa cells were infected with virus generated from pNL4.3.Luc.R-E- carrying either WT or K258R mutant IN. Infected cells were collected at 2 days post-infection. Abundance of (A) reverse transcription (RT) products and (B) 2-LTR circles was determined by qPCR and normalized to a housekeeping gene (n=4 and 6 respectively). (C) Proviral integration frequency was assayed using a nested PCR Alu-gag approach (n=7). (D) Luciferase activity was measured (RLU) and normalized by protein content to adjust for number of cells in input sample (n=8). (E) Steady state viral mRNA levels were measured by qPCR of infected cellular cDNA using primers against spliced *tat* message (n=3). All data is shown as a fold change relative to WT and is the average of the indicated number of independent biological replicates +/- SEs. Statistical significance was gauged by two-tailed paired t-test (\*p<0.05, \*\*p<0.01, \*\*\*p<0.001).

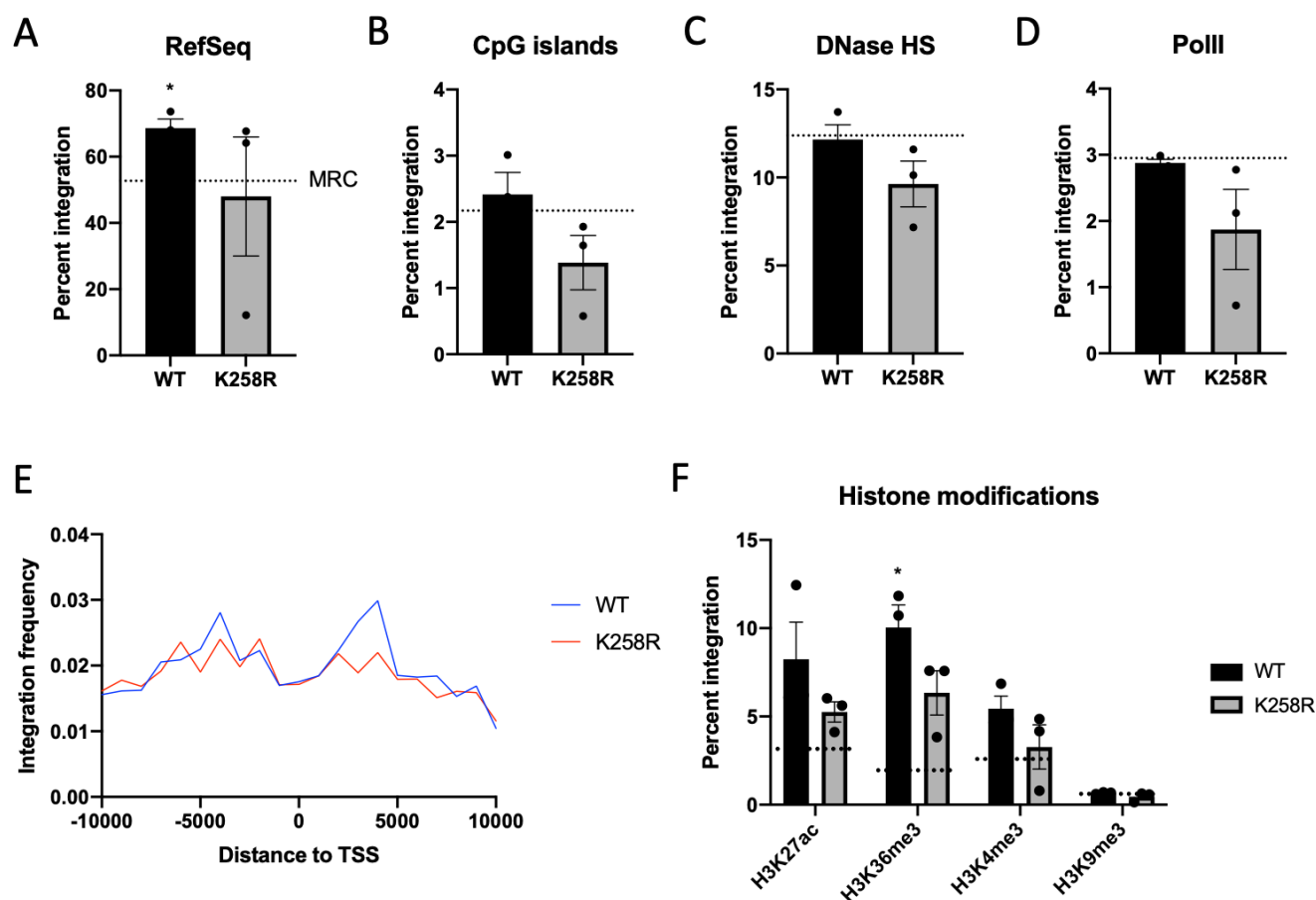


**Figure 2. The K258R mutation in IN alters integration site distribution.** Integration sites were mapped to the GRCh38 human reference genome assembly using Bowtie end-to-end alignment. Frequency of integrations falling within 1 kb of (A) RefSeq genes, (B) CpG islands, (C) DNase hypersensitivity sites and (D) RNA polymerase II binding sites was calculated using BedTools. The frequency of integrations expected to be located near these features by random chance (matched random control, MRC) is shown as a dashed line. (E) Distribution of integrations around transcription start sites (TSS). Integrations in a 10 kb window around TSS are shown. (F) Frequency of integrations within 1 kb of select pre-infection histone modification sites. Data shown is the average of three independent biological replicates +/- SEs. Statistical significance relative to MRC as gauged by a one-sample t-test is shown (\*  $p < 0.05$ ). Additional statistical analysis comparing the integration site pattern of WT and K258R mutant IN is shown in Table S4.

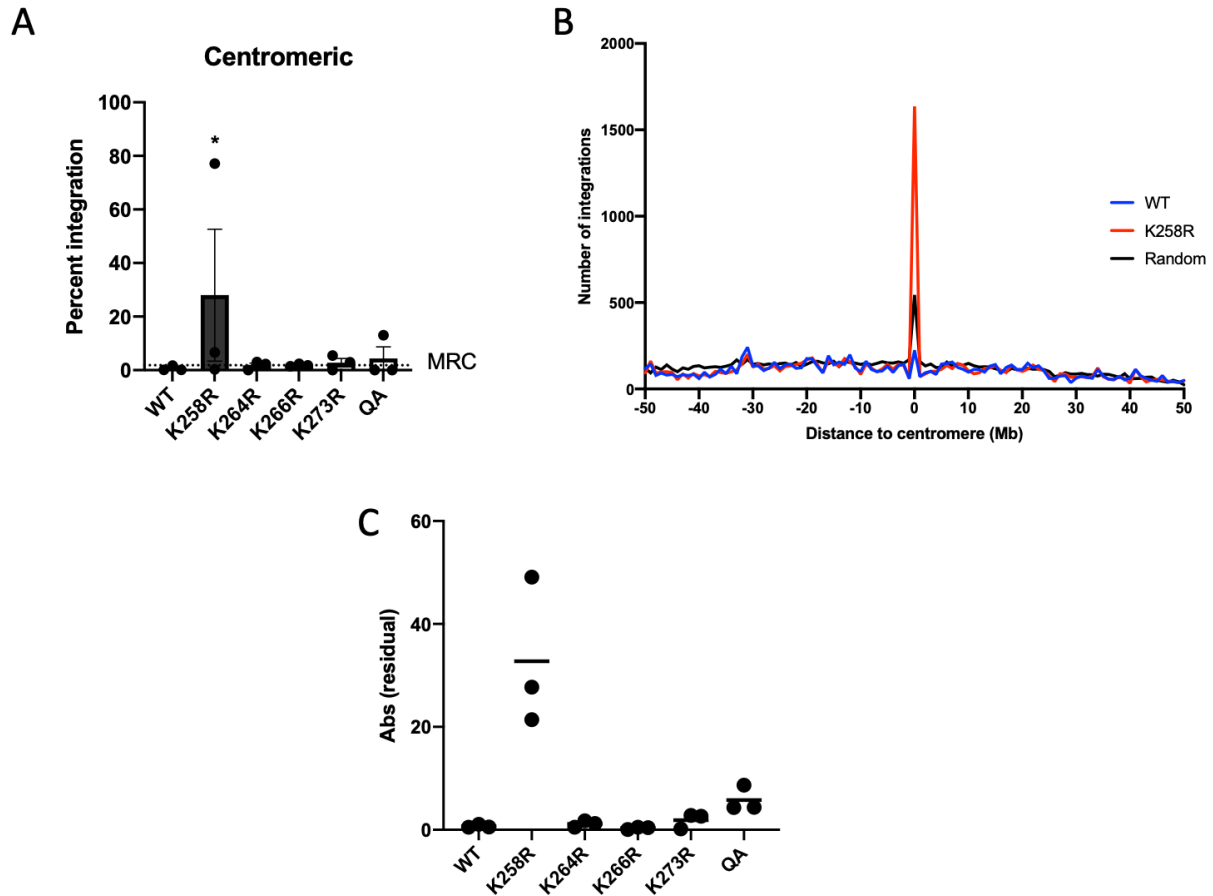


**Figure 3: K258R mutant HIV-1 IN biases integration toward centromeres.** (A) Number of integrations located in centromeric regions were normalized to total detected integration sites and are shown as a percent of the total. Integration frequency into centromeres in the matched random control (MRC) data set is shown as a dashed line. Data is shown as the average of three independent biological replicates +/- SEs. Statistical significance relative to MRC was calculated by one-way ANOVA corrected for multiple comparisons. (B) The distance to the nearest centromere was calculated for all WT and K258R mutant integration sites. A 50 Mb window flanking each centromere was segmented into 100 equal sized bins of 1 Mb. The number of integrations falling in each bin was quantified and is shown as a count (WT in black, K258R in red). (C) To assess variability of the altered integration centromere targeting phenotype we plotted the absolute residual from the mean for each independent trial. Statistical significance of variance was calculated using Levene's test (\*\*\*)  $p < 0.0001$ ,  $n=3$ ).



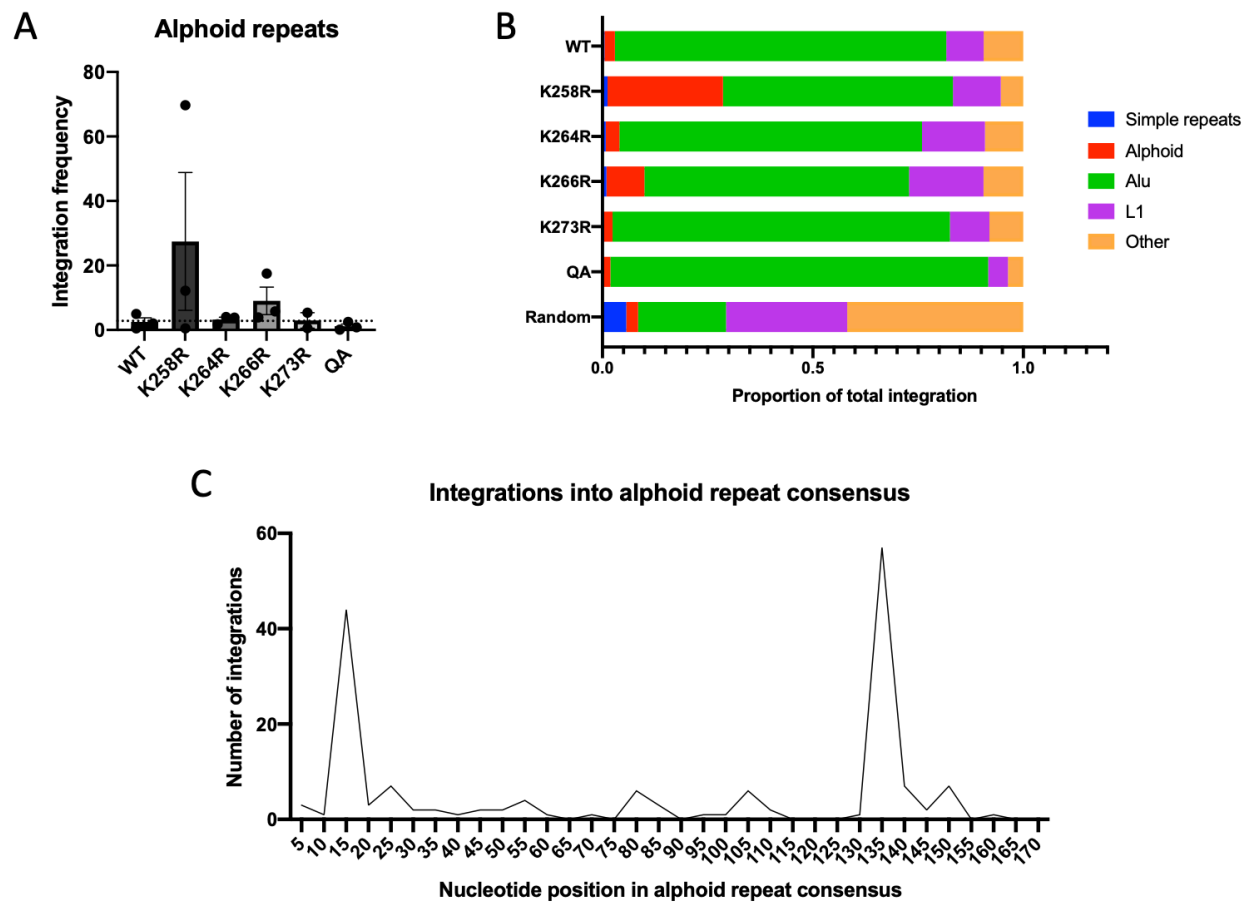


**Figure 4: Mapping of proviral integrations to repetitive regions in the human genome.** NGS reads from three independent biological replicate libraries were aligned to the RepeatMasker track from the UCSC genome browser. (A) The number of integrations mapping to alphoid DNA repeats was determined and normalized to the total number of mapped integrations and is shown as a percent of the total (n=3). The frequency with which integrations would be expected to fall in alphoid repeats if integration were random is shown as a dashed line (MRC). (B) The proportion of integrations that mapped to specific repeat elements relative to the total number of reads that mapped to the RepeatMasker track is shown. Only the most commonly targeted repeat elements are displayed. (C) Schematic of integration sites along the length of a single alphoid repeat. Unique host sequences immediately flanking each integration by the K258R mutant IN were aligned to an alphoid repeat consensus sequence (AJ131208.1) using Clustal Omega multiple sequence alignment. The consensus sequence was split into bins of 10 nucleotides and the number of integrations in each bin were counted. Shown are the integration counts falling in each bin summed over three replicates.

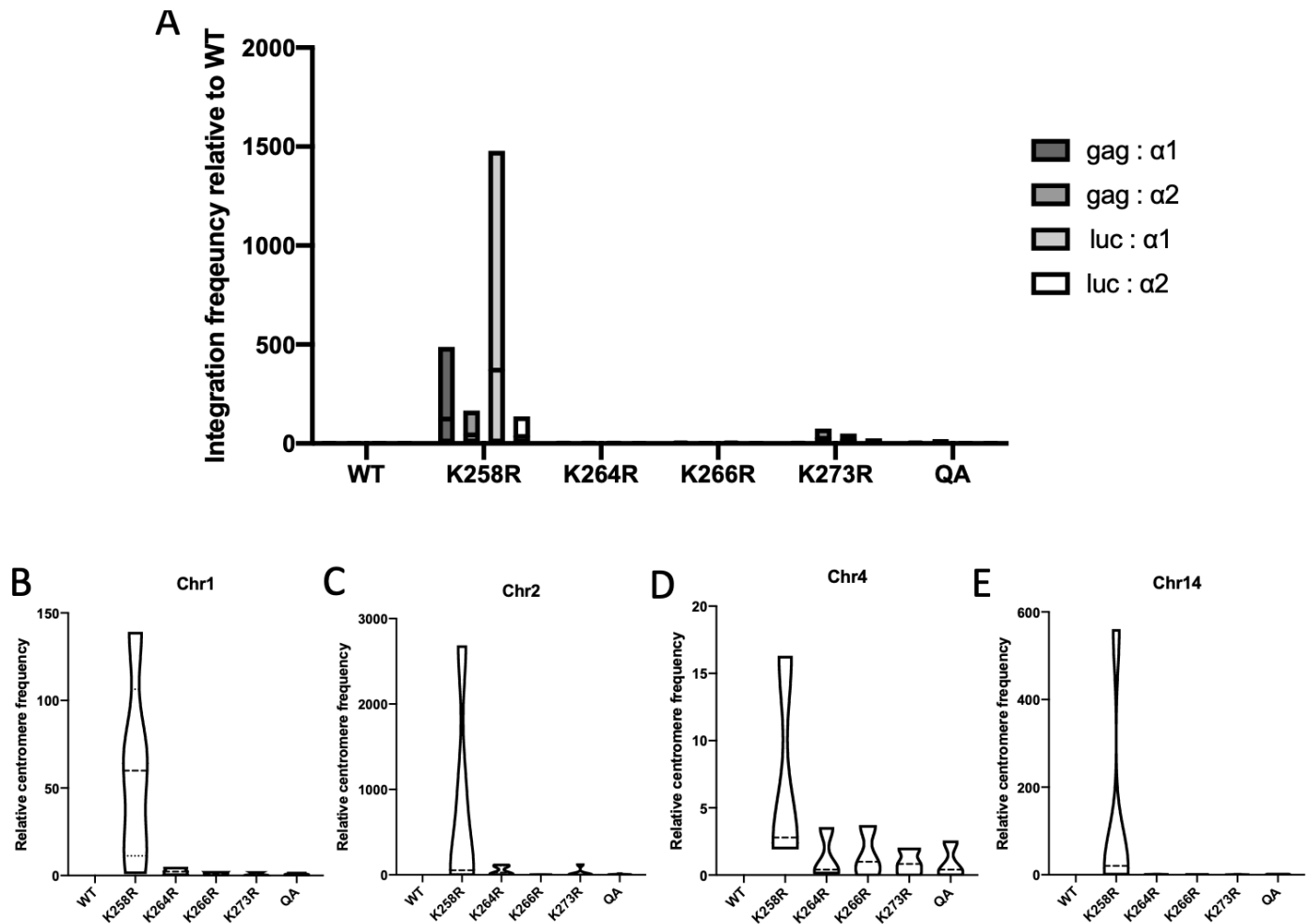


**Figure 5: Quantification of integration frequency into centromeric regions by qPCR methods.** (A) Integration into centromeric alphoid repeat DNA was quantified using a modified Alu-gag based nested PCR approach. Two unique primers were designed complementary to an alphoid repeat consensus sequence ( $\alpha 1$ ,  $\alpha 2$ ) and used instead of the typical Alu primer. Two primers at either end of the viral genome were used – either in the 5' end of gag or in the 3' UTR of the luciferase (luc) reporter gene. First nest PCR was performed with these four primer combinations. Shown are the results of a second nest quantitative PCR using LTR specific primers normalized to total integrated provirus levels as measured by Alu-gag PCR. Data from a minimum of three independent replicates is shown relative to WT as box plots to show the minimum, maximum and mean values. (B-E) Quantitative PCR using chromosome specific centromere primers. Viral LTR-host genome junctions were amplified and centromere content was subsequently quantified using qPCR with chromosome specific primers (see Table S1 for all primer sequences) and normalized to total integrated provirus levels as measured by Alu-gag PCR. Shown is the relative centromere content for each infected sample relative to WT from a minimum of three independent replicates presented as a violin plot to accurately represent the data distribution.